nature nanotechnology

ARTICLES

PUBLISHED ONLINE: 21 AUGUST 2011 | DOI: 10.1038/NNANO.2011.121

Self-assembly of self-limiting monodisperse supraparticles from polydisperse nanoparticles

Yunsheng Xia[1], Trung Dac Nguyen[2], Ming Yang[2], Byeongdu Lee[3], Aaron Santos[2], Paul Podsiadlo[4], Zhiyong Tang[1]*, Sharon C. Glotzer[2,5]* and Nicholas A. Kotov[2,5]*

Nanoparticles are known to self-assemble into larger structures through growth processes that typically occur continuously and depend on the uniformity of the individual nanoparticles. Here, we show that inorganic nanoparticles with non-uniform size distributions can spontaneously assemble into uniformly sized supraparticles with core–shell morphologies. This self-limiting growth process is governed by a balance between electrostatic repulsion and van der Waals attraction, which is aided by the broad polydispersity of the nanoparticles. The generic nature of the interactions creates flexibility in the composition, size and shape of the constituent nanoparticles, and leads to a large family of self-assembled structures, including hierarchically organized colloidal crystals.

Nanoparticles can assemble into larger, microscale structures under conditions of strongly anisotropic interactions[1–4] when prepared as binary mixtures of monodisperse nanoparticles[5,6], or when highly monodisperse with mostly isotropic repulsion[7,8]. The faceted shapes of crystalline nanoparticles, in particular, facilitate attraction along specific axes and increase the complexity of the produced structures[9–19]. For the majority of nanoparticle assemblies forming spontaneously in bulk solutions[20–23], self-organization occurs continuously until the components are exhausted and the nanoparticles form a dry crystal, complex solid or precipitate. In many cases the formation is governed by strong non-equilibrium processes, so the products depend on kinetic factors and especially on the uniformity of the individual nanoparticles.

A self-limiting, self-assembly process that involves non-uniform inorganic nanoparticles, and results in highly ordered terminal structures, would be conceptually different from currently known self-organization reactions. If such assemblies could be fabricated easily and inexpensively, they would be of use in applications ranging from transformation optics to photovoltaics and drug delivery. Similar to the process of layer-by-layer assembly, which is based on the self-limiting growth of individual monolayers[24], self-limited nanoparticle superstructures would provide greater versatility in the produced assemblies, and both relax the requirements for, and broaden the choice of, constituent building blocks. Because self-limiting structures are common in biological systems, their realization using inorganic nanocrystals might lead to unexpected parallels between the world of inorganic colloids and biomacromolecules, and could potentially lead to inorganic assemblies with complexity rivalling those of biological structures. Here, using inorganic nanoparticles of CdSe, CdS, ZnSe and PbS, we show that such assembly is possible and requires only competing, isotropic forces. The simple, but generic, assembly mechanism can create complex semiconductor and metal–semiconductor supraparticles displaying a significant degree of geometrical uniformity and geometrical shapes both with and without anisotropy.

Assembly of CdSe nanoparticles into supraparticles

CdSe nanoparticles stabilized by short and highly charged citrate anions (see Supplementary Methods) were adopted as an initial model system because of their well-established optical properties, and the possibility to combine strong electrostatic and van der Waals interactions. The nanoparticles are polycrystalline (Supplementary Fig. S1) and have irregular spherical shapes with no pronounced facets or anisometry. Growth and assembly of CdSe nanoparticles occurred simultaneously in aqueous solution at 80 °C. When necessary, the reaction was slowed down or interrupted by cooling the reaction media. Within 20 min of the reaction, one can clearly observe supraparticles with a median diameter $d_{SP} = 22 \pm 2.4$ nm and size distribution $\delta_{SP} = 11\%$, as determined by transmission electron microscopy (TEM) (Fig. 1c and Table 1). In reference to their approximate TEM diameter, these supraparticles will be denoted CdSe-20. The constituent nanoparticles have an average diameter $d_{NP} = 2.9 \pm 0.7$ nm and TEM size distribution $\delta_{NP} = 25\%$ (Fig. 1c, Table 1). Note the surprising difference between the low polydispersity of the supraparticles and the relatively high polydispersity of the constituent nanoparticles, which is indicative of a self-organization process that is conceptually different from those previously reported[5–23]. No tendency to produce larger and/or smaller aggregates or precipitates was observed.

As the reaction progresses, the supraparticles grow in diameter to 33 ± 2.5 nm, 42 ± 3.5 nm and 49 ± 4.1 nm for 120, 1,080 and 2,400 min reaction times, respectively (Fig. 1). Approximating the TEM diameters, we refer to these samples as CdSe-30, CdSe-40 and CdSe-50. During the reaction, the nanoparticles within the supraparticles increase in size to 3.5 ± 0.80 nm in CdSe-30, 4.5 ± 1.1 nm in CdSe-40 and 5.4 ± 1.4 nm in CdSe-50. The reduction of the polydispersity in the supraparticles (8–10%) compared with the individual units of which they are comprised (25–30%) occurs in all samples (Fig. 1f,i,l), as confirmed by several independent experimental techniques (Table 1). It is important to highlight the fact that the monodispersity of the supraparticle is high enough to produce nearly perfect colloidal crystals (Fig. 1m), which provides

[1]National Center for Nanoscience and Technology, 11 Beiyitiao, Zhongguancun, Beijing, 100190, China, [2]Department of Chemical Engineering, University of Michigan, Ann Arbor, Michigan 48109, USA, [3]Advanced Photon Source, Argonne National Laboratory, 9700 S. Cass Avenue, Argonne, Illinois 60439, USA, [4]Center for Nanoscale Materials, Argonne National Laboratory, 9700 S. Cass Avenue, Argonne, Illinois 60439, USA, [5]Department of Materials Science and Engineering, University of Michigan, Ann Arbor, Michigan 48109, USA. *e-mail: zytang@nanoctr.cn; sglotzer@umich.edu; kotov@umich.edu

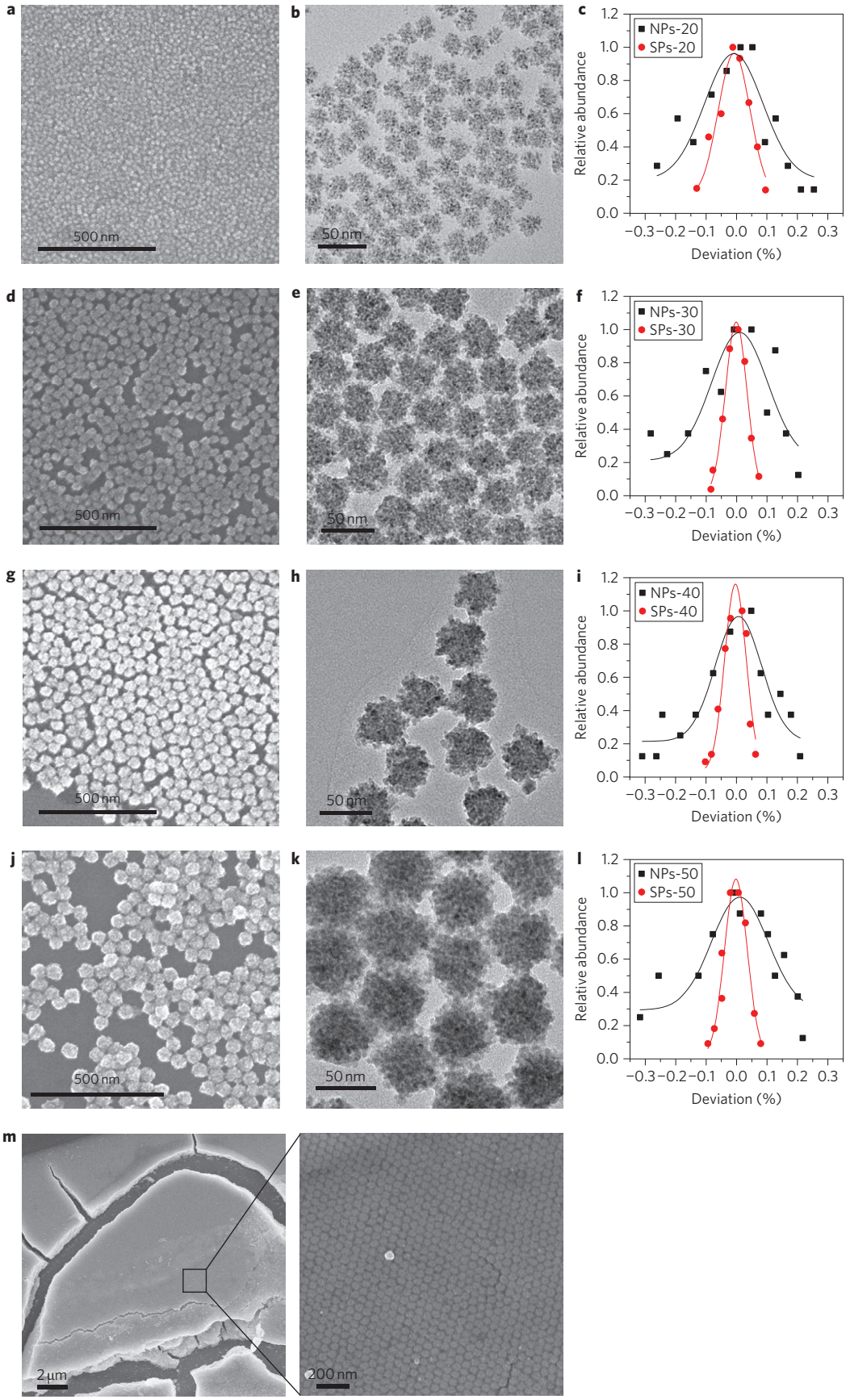

Figure 1 | Electron microscopy and size distribution for supraparticles. a–l, EM (**a**,**d**,**g**,**j**), TEM (**b**,**e**,**h**,**k**) images and size distribution (**c**,**f**,**i**,**l**) of four CdSe supraparticle samples obtained at different reaction times: 20 min, CdSe-20 (**a–c**); 120 min, CdSe-30 (**d–f**); 1,080 min, CdSe-40 (**g–i**); 2,400 min, CdSe-50 (**j–l**). **m**, SEM images of colloidal crystals made of CdSe supraparticles.

Table 1 | Sizes and size distributions of supraparticles and their constituent nanoparticles.

Nanoparticle subunits					Supraparticles			
Samples	d_{NP}^{TEM} (nm)	$d_{NP}^{UV\text{-}vis}$ (nm)	d_{NP}^{SAXS*} (nm)	s.d. $\delta_{NP}{}^{\dagger}$ (%)	d_{SP}^{TEM} (nm)	d_{SP}^{DLS} (nm)	d_{SP}^{SAXS} (nm)	s.d. $\delta_{SP}{}^{\dagger}$ (%)
CdSe-20	2.9	2.5	-	25	22.1	22.5	-	11
CdSe-30	3.5	3.8	3.9	23	32.8	42.6	37.2	7.6
CdSe-40	4.5	4.7	5.5	25	42.2	51.8	45.6	8.2
CdSe-50	5.4	5.6	6.8	26	49.2	60.2	49.0	8.3

Superscript denotes the experimental method used for the evaluation of the diameter of nanoparticles (NPs) and supraparticles (SPs). *Inter-nanoparticle distance (centre-to-centre). $^{\dagger}d_{NP}$ and d_{SP} represent the diameters of nanoparticles and supraparticles, respectively. δ_{NP} and δ_{SP} represent the standard deviations (s.d.) of nanoparticles and supraparticles, respectively. δ_{NP} and δ_{SP} were calculated based on 100 measurements taken at different locations on TEM grids.

both a benchmark for the supraparticle size uniformity and a pathway to a new family of materials[5–11,13–19]. In this respect, the short length of citrate as nanoparticle stabilizer is significant. Long-chain organic stabilizers used before strongly impede charge transport between the particles in colloidal crystals.

The assembly of supraparticles occurs when monomers producing CdSe are present in the media. Their contribution is taken into account via the growth of constituent nanoparticles. No experimental evidence was found that the monomers produce supraparticles independently, which would certainly result in a much wider size distribution, similar to that of individual nanoparticles. The depletion of the monomers cannot be responsible for supraparticle monodispersity because there is a great difference in monomer concentration for, say, CdSe-20 and CdSe-50, but little effect on monodispersity is observed.

We note that some reduction in the size distribution is expected from the 'central limit theorem' (CLT), which states that the standard deviation of the mean of a set (that is, the supraparticles) of random variables (nanoparticles) will be reduced by the square root of the number of variables in the set[25]. Here, the convergence of the assembled particles to a specific diameter of the supraparticle must additionally involve interactions within the supraparticles and cannot be explained exclusively by CLT.

To ascertain that the assembly process takes place in solution rather than on the substrates during drying, dynamic light scattering (DLS) experiments were performed to directly measure the sizes of supraparticles in solution (Supplementary Fig. S3). The average hydrodynamic diameters for the CdSe-20, CdSe-30, CdSe-40 and CdSe-50 samples are 23, 43, 52 and 60 nm (Table 1), respectively, in agreement with TEM measurements, despite some apparent enlargement due to a hydration layer and a stronger contribution of larger particles to the DLS signal[26].

The intermediate stages of the assembly process were monitored at 40 °C. We observed that CdSe first nucleates and grows to form individual nanoparticles (Fig. 2a). Next, some nanoparticles assemble into elongated aggregates (Fig. 2b) which later evolve into loose, more isometric clusters comprising 15–25 nanoparticles. Finally, the intermediate clusters undergo compaction to produce denser and more monodisperse supraparticles (Fig. 2d). The same sequence of assembly stages, that is, individual nanoparticle → loose elongated aggregates → larger aggregates → compact spherical uniform supraparticles, is also deduced from the combination of DLS and ultraviolet–visible (UV–vis) absorption data cumulatively expressed in Fig. 2e. The size ratio d_{SP}/d_{NP} initially increases following the transition from individual nanoparticles to loose clusters. After that, d_{SP}/d_{NP} decreases when the clusters compactify. Powder X-ray diffraction results (Supplementary Fig. S4) indicate that despite densification, nanoparticles in the supraparticles retain their individuality: merger of crystalline lattices does not take place[27].

Core–shell structure of monodisperse supraparticles

Detailed information about the structure of the supraparticles (Fig. 2f,g,h) can be obtained by synchrotron small-angle X-ray scattering (SAXS). In the small-q region ($q < 0.03$ Å^{-1}), a distinct scattering pattern is observed with the first minimum at $q = 0.0236$, 0.0202 and 0.0182 Å^{-1} for CdSe-30, CdSe-40 and CdSe-50, respectively. The scattering behaviour confirms high monodispersity in the large ensemble of supraparticles in solution. The corresponding diameters of the dispersed supraparticles calculated from SAXS data, namely 37 ± 0.4, 46 ± 0.5 and 49 ± 0.5 nm (Supplementary Table S1), match well with the TEM, scanning electron microscopy (SEM) and DLS data (Fig. 1, Table 1) for CdSe-30, CdSe-40 and CdSe-50, respectively.

From the inflection points (or broad diffraction peaks) in Fig. 2f one can calculate inter-nanoparticle centre-to-centre distances within the supraparticles. For the CdSe-30, CdSe-40 and CdSe-50 samples these distances are estimated to be 3.9 ± 0.2, 5.5 ± 0.2 and 6.8 ± 0.4 nm, respectively. These values are slightly larger than the average d_{NP} (Table 1) by ~1.5 nm, which is comparable to the expected thickness of two organic shells of citrate ions coating the nanoparticles. There are no specific peaks that could be attributed to ordering of nanoparticles within the supraparticles, consistent with their high degree of polydispersity (Fig. 1a).

The region of larger q corresponds to the contribution of individual nanoparticles to the scattering pattern. There are no characteristic oscillations observed for $q > 0.1$ Å^{-1}, confirming that individual nanoparticles are significantly more polydisperse than their assemblies; this is in excellent agreement with data in Table 1 obtained by imaging, scattering and spectroscopic techniques.

We observe that drying does not change the supraparticles substantially (Fig. 2f). The size of the supraparticles is reduced only by ~10% (Fig. 2f) with average diameters of 33 ± 0.3 nm (CdSe-30), 40 ± 0.4 nm (CdSe-40) and 42 ± 0.4 nm (CdSe-50), consistent with dense packing of nanoparticles in supraparticles. Drying most likely removes water predominantly from the interstitial regions between the nanoparticles, resulting in a slight rearrangement of them within the supraparticles.

Fitting of SAXS curves yields an average of 280 nanoparticles in a single supraparticle in the CdSe-50 sample (Fig. 2g). Interestingly, we observe a distinct gradient in packing density inside the supraparticles, with a more loosely packed core and more densely packed outer shell of nanoparticles (Fig. 2h). In the CdSe-50 sample, we measured a shell thickness of ~5 nm (Fig. 2h, Supplementary Fig. S9b), suggesting the shell is a monolayer comprised of 5.4-nm-diameter nanoparticles.

The fact that the polydisperse nanoparticles assemble into monodisperse, spherical supraparticles, rather than aggregates or precipitates with a broad size distribution and/or irregular shapes, suggests that the agglomeration of the nanoparticles here is both thermodynamically controlled and self-limiting. Considering the high negative charge of the citrate-stabilized nanoparticles, it is logical to assume that electrostatic interactions play an important role in the self-limiting behaviour of the otherwise attractive nanoparticles. Indeed, investigation of the evolution of the electrokinetic ζ-potential during the formation and maturation of supraparticles (Fig. 2e) shows that, although initially small (~0 to −5 mV), it increases substantially as the supraparticles grow, and stabilizes when the supraparticles reach the stage of compact assemblies. We therefore propose that the reason for the ultimate cessation of supraparticle

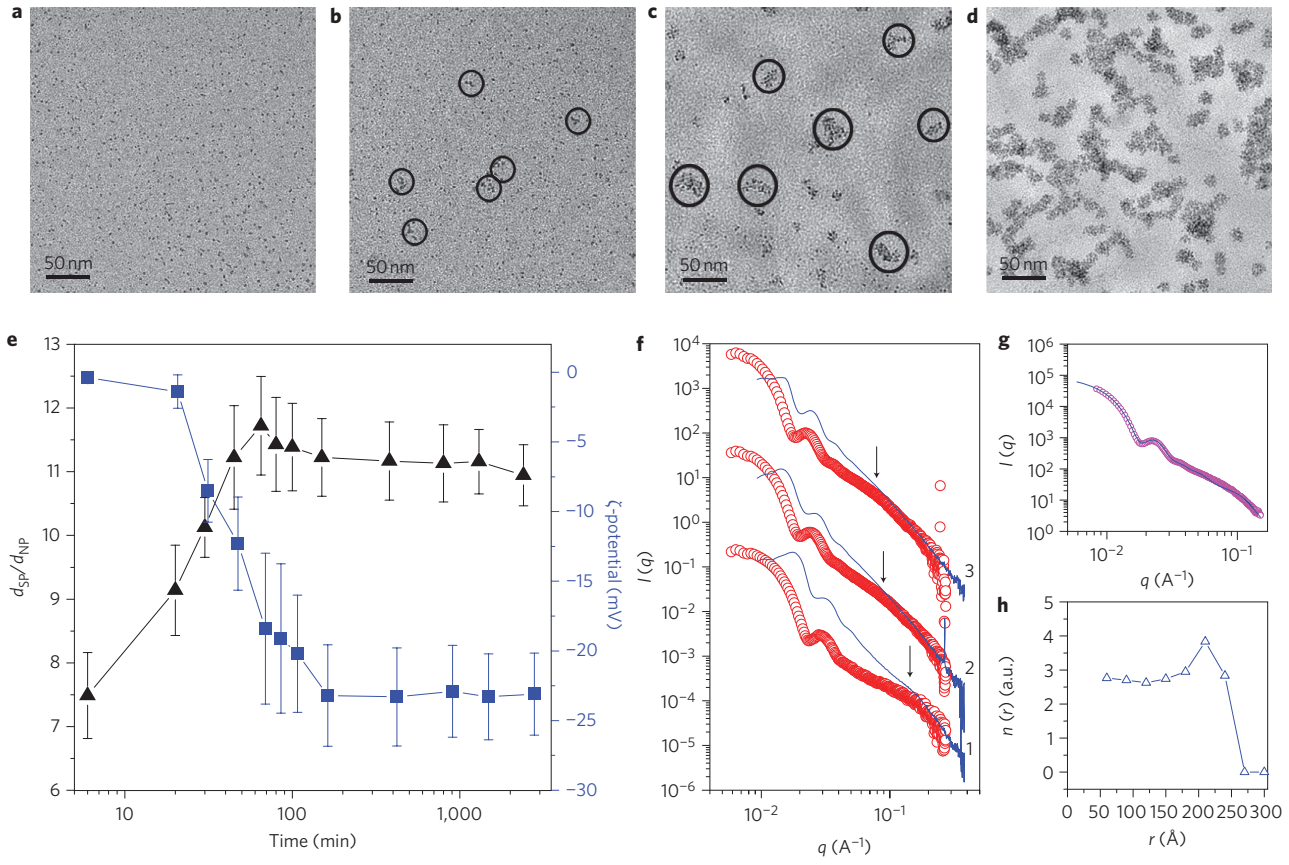

Figure 2 | Intermediate stages of formation of supraparticle at 40 °C and detailed structural characterization of supraparticles. a–d, Stages of formation at 5 min (**a**), 9 min (**b**), 15 min (**c**) and 19 min (**d**). **e**, Experimental dependence of d_{SP}/d_{NP} and the electrokinetic ζ-potential on reaction times. d_{SP} and d_{NP} were measured by DLS and UV-vis spectroscopy, respectively, and electrokinetic ζ-potential was measured by DLS. **f**, SAXS curves for CdSe-30 (1), CdSe-40 (2) and CdSe-50 (3) supraparticles. Red and blue lines represent solution and dried samples, respectively. Inflection points are marked by arrows. **g**, Measured data for CdSe-50 in solution (magenta) and calculated curves from core–shell supraparticle model (blue). **h**, Radial distribution of the number of subunits for the core–shell supraparticle model for CdSe-50.

growth is the strong electrostatic repulsion between supraparticles and between supraparticles and nanoparticles, which must ultimately balance the van der Waals attraction between nanoparticles. Note that the electrostatic charge on the supraparticles arises from the intrinsic charges of the individual nanoparticles and at interfaces between nanoparticles, including those inside the supraparticles. The electroneutrality assumption for the surfaces of constituent nanoparticles is not necessarily applicable, because the inter-nanoparticle gaps are too narrow to develop a proper double electric layer[28,29].

Formation mechanism of monodisperse supraparticles

Further studies were carried out using computer simulation, allowing many different combinations of forces, nanoparticle shapes and polydispersities to be tested, as well as assembly conditions that might be reasonably expected in this system. Although the effects of particle size polydispersity on the uniformity and ordering of self-assembled structures have been reported in previous computational studies[30–34], few investigations (if any) have been carried out on the simulation of nanoparticle assembly into uniformly sized clusters. Brownian dynamics was used to simulate systems of nanoparticles in a three-dimensional cubic box with periodic boundary conditions at constant volume and temperature (see Supplementary Materials, Computer Simulations, for details). A Lennard-Jones 12-6 potential was used to model the van der Waals attraction between nanoparticles, and a screened Coulomb potential was used for electrostatic interactions (Supplementary Information, Simulation Model). Because the net charge of the supraparticles increases with their size (Fig. 2e), the repulsion strength between nanoparticles (free or clustered) and supraparticles was set to be proportional to the supraparticle volume. The model also stipulates that the repulsion strength and screening length of the Coulomb interaction between nanoparticles within the core of a supraparticle is greater than between those in the outer layer, because the dielectric constant of the medium inside the supraparticle (ε_{CdSe} = 8.0–9.0) is smaller than that outside ($\varepsilon_{solution}$ = 80.0). As a result, the electrostatic repulsion strength is not constant throughout a simulation as in conventional studies, but instead depends on the changing location of the nanoparticles as the simulation proceeds. Based on all simulation runs, we found that the case of spherical nanoparticles with δ_{NP}^{simul} = 20%, interacting only via repulsive electrostatic and attractive van der Waals forces, describes the assembly process nearly perfectly.

The simulated systems of nanoparticles with δ_{NP}^{simul} = 0–30% were found to follow the same assembly stages as in experiments: individual nanoparticle → loose elongated aggregates → larger aggregates → compact spherical uniform supraparticles (compare Fig. 3a and Fig. 2a–d). At the final stage, the monodisperse supraparticles are close to spherical in shape. Some 'spikiness' of the real supraparticles compared with the simulated supraparticles (Fig. 1 versus Fig. 3a) is probably due to the fact that nanoparticles can continue to grow after their assembly into supraparticles, especially those in the outer shell of a supraparticle. This growth should be anisotropic owing to a higher concentration of ions

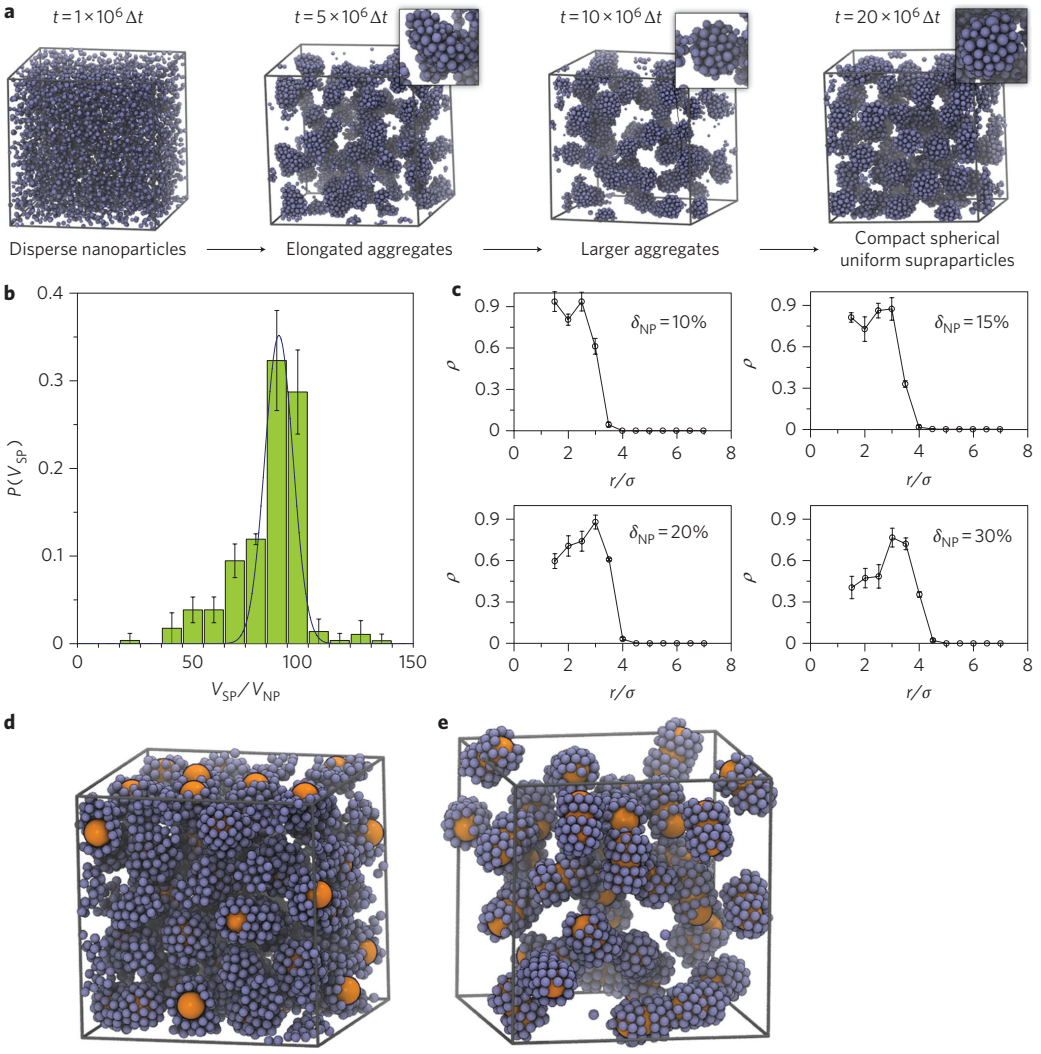

Figure 3 | Computer simulation results. a, The four stages of supraparticle self-assembly as a function of time. The asphericity parameter of the simulated supraparticles in the final stage of assembly is 0.014±0.006. **b**, Size distribution of the simulated supraparticles assembled from nanoparticles with $\delta_{NP} = 20\%$, fitted by a 7% standard deviation Gaussian distribution (blue curve). $V_{NP} = \pi\sigma^3/6$ is the average nanoparticle volume. **c**, Particle density versus distance r from supraparticle centre, scaled by nanoparticle average diameter σ. **d**, Computer simulation of core–shell supraparticles self-assembled from CdSe nanoparticles (blue) and preformed gold nanospheres (orange). **e**, Computer simulation of core–shell supraparticles self-assembled from CdSe nanoparticles (blue) and pre-formed gold nanorods (orange).

outside the supraparticles, with a tendency for radially outward growth of nanoparticles in the outer shell of the supraparticles. Once a supraparticle reaches a size where the electrostatic repulsion energy between nanoparticles in the supraparticle and the newly arrived nanoparticles outside the supraparticle equals the attractive energy associated with van der Waals interactions, the agglomeration stops (Supplementary Information, Computer Simulations). Importantly, we find that self-limiting behaviour occurs only if the electrostatic repulsion increases monotonically with the volume of the supraparticle being assembled. Otherwise, nanoparticles continue to aggregate, regardless of screening length.

Supraparticles assembled *in silico* from nanoparticles with $\delta_{NP}^{simul} = 20\%$ exhibit a sharp peak in cluster size distribution (Fig. 3b) at a single value of V_{SP}^{simul}, reproducing the size monodispersity observed in experiments. The size distribution of the simulated supraparticles is fitted well by a normal distribution with standard deviation of 7% (Fig. 3b), which is very close to the experimentally observed size distribution (Table 1). Observations of the plateau in system potential energy versus time and of the small fluctuation in the final average number of nanoparticles per supraparticle (Supplementary Fig. S12a) confirm our hypothesis that the system of stable, monodisperse supraparticles is not kinetically trapped, but is instead in a thermodynamic equilibrium state. To further ensure that the supraparticles are not a consequence of kinetic effects, we gradually increased the nanoparticle density from ~0.01 to ~0.1 to reduce the average distance between the supraparticles, and observed that the supraparticles do not merge into larger supraparticles, as would be the case if the observed configuration were not in thermodynamic equilibrium. It is also important to note that when analogous simulations were run with different nanoparticle geometries or different forces (spherical and tetrahedral nanoparticles, with and without dipole interactions, and with and without polydispersity; Supplementary Fig. S15), the geometry of the resulting agglomerates was markedly different from monodisperse spherical supraparticles.

Our simulations also reproduce the internal structure of the supraparticles inferred from the TEM and SAXS measurements. The core–shell structure of the supraparticles clearly emerges for $\delta_{NP}^{simul} = 20$–30% (Fig. 3c). For $\delta_{NP}^{simul} = 20\%$, the simulated packing densities in the core and in the shell are 74±7% and

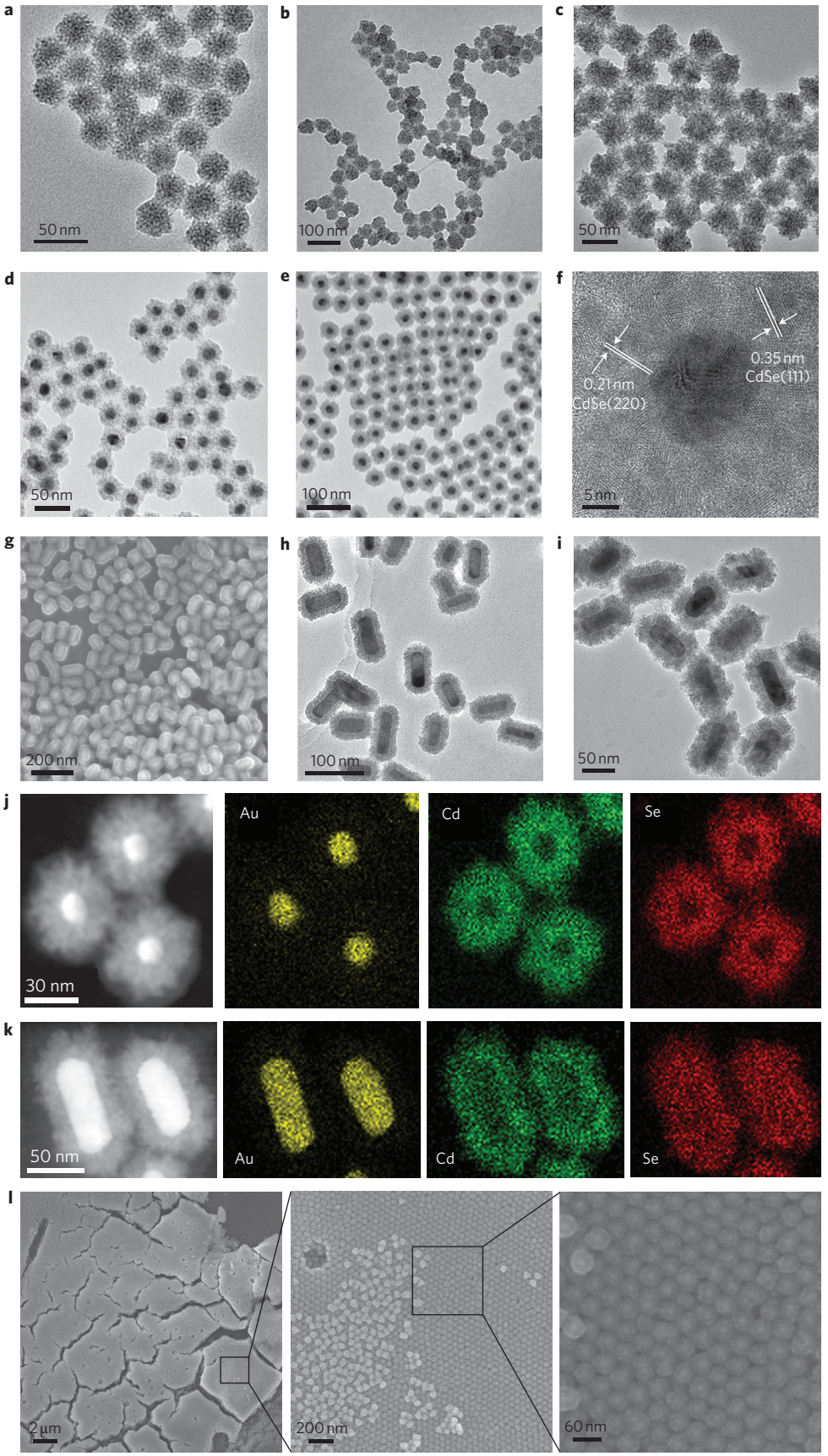

Figure 4 | Analogous supraparticle assemblies from different materials. a–i, TEM and SEM images from CdS (**a**), ZnSe (**b**) and PbS (**c**) supraparticles, and Au-sphereCdS (**d**), Au-sphereCdSe (**e**,**f**), Au-rodCdS (**g**,**h**) and Au-rodCdSe (**i**) core–shell supraparticles. **j**,**k**, Images of high-angle annular dark-field scanning TEM and energy-dispersive X-ray elemental mapping from Au-sphereCdSe (**j**) and Au-rodCdSe (**k**) core–shell supraparticles. **l**, SEM image of colloidal crystals from Au-sphereCdSe supraparticles.

89 ± 5%, respectively; these values correlate well with experiments for the CdSe-50 case. The strong electrostatic repulsion inside the supraparticles gives rise to the loosely packed core of the supraparticles. Additionally, the remarkable nanoparticle polydispersity leads to nanoparticle rearrangement within the supraparticles such that smaller nanoparticles pack in the outer shell and larger nanoparticles concentrate in the core (Supplementary Fig. S13b). Further, we observe that the nanoparticles in the shell are more polydisperse than those in the core, which explains the surprisingly high packing density in the shell (Supplementary Fig. S13b).

The forces leading to the formation of monodisperse supraparticles are general and the approach should be applicable to a large variety of 'imperfect' nanoparticles from other materials. Indeed, similar supraparticles form from group II–VI semiconductors such as CdS and ZnSe, and from group IV–VI semiconductors such as PbS (Fig. 4a–c). Considering the simple balance of forces, we further propose that similar self-limiting structures might form around pre-existing cores. In practice, such cores may be realized through like-charged particles capable of strong van der Waals attraction with nanoparticles in the solution. We note that this strategy is opposite to the often-used strategy of using nanocolloids of opposite charge as core particles[35,36]. To test our hypothesis, we added gold nanoparticles with $d < d_{SP}$ stabilized by citrate with an electrokinetic potential of −39.4 mV to a solution of CdSe nanoparticles before their assembly into supraparticles. We indeed observed the assembly of hybrid supraparticles with a single gold core surrounded by CdSe nanoparticles (Fig. 4d–f). The nature of the core–shell structure of these hybrid supraparticles can be confirmed by elemental mapping of the particles (Fig. 4j). The supraparticles are highly monodisperse and their formation is also governed by the balance of van der Waals attraction between CdSe nanoparticles and gold particle 'cores', and electrostatic repulsion as verified by computer simulation (Fig. 3d). The use of preformed cores offers the possibility to further increase the complexity of supraparticles and can lead to easy-to-make superstructures with a rich variety of geometries and functionalities. The produced metal–semiconductor supraparticles can self-assemble further into colloidal crystals, producing unique hierarchical assemblies and multiple applications (Fig. 4l)[17,18]. A comparison of complex supraparticles and superstructures made by the oriented attachment of nanoparticles, for instance as carried out by Peng and colleagues[21], shows a very different mechanism for the assembly as well as the morphology of the assembled products. Further comparison with classical core–shell quantum dots could also be instructive, revealing that the complex core–shell supraparticles have very different formation pathway, characteristic size, and forces providing structural stability, as well as different potential areas of application from any examples of core–shell quantum dots.

Inorganic supraparticles versus virus particles

We also found that anisotropic gold nanorods yield equally monodisperse cylindrical supraparticles, both in experiments (Fig. 4g–i,k) and simulations (Fig. 3e). Remarkably, both the spherical and rod-like core–shell supraparticles bear some resemblance to such biological superstructures as viral capsids, in which protein capsomers form a single-layer shell around a DNA or RNA core. For example, the cowpea mosaic virus is a spherical, 28 nm supraparticle with an icosahedral structure assembled by 60 protein subunits[37], while influenza, rabies and other viruses are prolate, or rod-like supraparticles of similar size and unit number. Note that some viruses, such as the HIV virus, do not exhibit geometrically perfect packing. Our work demonstrates that nanoparticles can organize with similar levels of complexity as viruses, albeit following a wholly different assembly pathway without any lock-and-key interactions specific for proteins and other biomolecules, but instead by a simple balance of generic coulombic and van der Waals forces. The self-limiting state also distinguishes the supraparticles found here from self-limiting, 'magic number' clusters known for monodisperse nano- and microparticles[38,39]. Supraparticle assembly can be further exploited for the experimental engineering of sophisticated nanoscale systems, including reconfigurable assemblies, combined with their design and testing *in silico*, and hierarchically organized colloidal crystals of supraparticles will open the door to simple manufacturing pathways of complex macroscale hybrid materials and devices.

Received 14 March 2011; accepted 28 June 2011;
published online 21 August 2011; corrected online 26 August 2011

References

1. Tang, Z., Kotov, N. A. & Giersig, M. Spontaneous organization of single CdTe nanoparticles into luminescent nanowires. *Science* **297,** 237–240 (2002).
2. Tang, Z., Zhang, Z. L., Wang, Y., Glotzer, S. C. & Kotov, N. A. Self-assembly of CdTe nanocrystals into free-floating sheets. *Science* **314,** 274–278 (2006).
3. Srivastava, S. *et al.* Light-controlled self-assembly of semiconductor nanoparticles into twisted ribbons. *Science* **327,** 1355–1359 (2010).
4. Glotzer, S. C. & Solomon, M. J. Anisotropy of building blocks and their assembly into complex structures. *Nature Mater.* **6,** 557–562 (2007).
5. Dong, A., Chen, J., Vora, P. M., Kikkawa, J. M. & Murray, C. B. Binary nanocrystal superlattice membranes self-assembled at the liquid–air interface. *Nature* **466,** 474–477 (2010).
6. Shevchenko, E. V., Talapin, D. V., Kotov, N. A., O'Brien, S. & Murray, C. B. Structural diversity in binary nanoparticle superlattices. *Nature* **439,** 55–59 (2006).
7. Murray, C. B., Kagan, C. R. & Bawendi, M. G. Synthesis and characterization of monodisperse nanocrystals and close-packed nanocrystal assemblies. *Annu. Rev. Mater. Sci.* **30,** 545–610 (2000).
8. Pileni, M. P. Nanocrystal self-assemblies: fabrication and collective properties. *J. Phys. Chem. B* **105,** 3358–3371 (2001).
9. Sun, S., Murray, C. B., Weller, D., Folks, L. & Moser, A. Monodisperse FePt nanoparticles and ferromagnetic FePt nanocrystal superlattices. *Science* **287,** 1989–1992 (2000).
10. Nikoobakht, B., Wang, Z. L. & El-Sayed, M. A. Self-assembly of gold nanorods. *J. Phys. Chem. B* **104,** 8635–8640 (2000).
11. Sun, Y. & Xia, Y. Shape-controlled synthesis of gold and silver nanoparticles. *Science* **298,** 2176–2179 (2002).
12. Cölfen, H. & Mann, S. Higher-order organization by mesoscale self-assembly and transformation of hybrid nanostructures. *Angew. Chem. Int. Ed.* **42,** 2350–2365 (2003).
13. Talapin, D. V. *et al.* CdSe and CdSe/CdS nanorod solids. *J. Am. Chem. Soc.* **126,** 12984–12988 (2004).
14. Niederberger, M. & Cölfen, H. Oriented attachment and mesocrystals: non-classical crystallization mechanisms based on nanoparticle assembly. *Phys. Chem. Chem. Phys.* **8,** 3271–3287 (2006).
15. Tao, A., Sinsermsuksakul, P. & Yang, P. Tunable plasmonic lattices of silver nanocrystals. *Nature Nanotech.* **2,** 435–440 (2007).
16. Zhang, Z., Tang, Z., Kotov, N. A. & Glotzer, S. C. Simulations and analysis of self-assembly of CdTe nanoparticles into wires and sheets. *Nano. Lett.* **7,** 1670–1675 (2007).
17. Lee, J. S., Shevchenko, E. V. & Talapin, D. V. Au–PbS core–shell nanocrystals: plasmonic absorption enhancement and electrical doping via intra-particle charge transfer. *J. Am. Chem. Soc.* **130,** 9673–9675 (2008).
18. Jones, M. R. *et al.* DNA–nanoparticle superlattices formed from anisotropic building blocks. *Nature Mater.* **9,** 913–917 (2010).
19. Quan, Z. & Fang, J. Superlattices with non-spherical building blocks. *Nano Today* **5,** 390–411 (2010).
20. Maye, M. M. *et al.* Size-controlled assembly of gold nanoparticles induced by a tridentate thioether ligand. *J. Am. Chem. Soc.* **125,** 9906–9907 (2003).
21. Narayanaswamy, A., Xu, H., Pradhan, N. & Peng, X. Crystalline nanoflowers with different chemical compositions and physical properties grown by limited ligand protection. *Angew. Chem. Int. Ed.* **45,** 5361–5364 (2006).
22. Zhuang, J., Wu, H., Yang, Y. & Cao, Y. C. Supercrystalline colloidal particles from artificial atoms. *J. Am. Chem. Soc.* **129,** 14166–14167 (2007).
23. Liu, K. *et al.* Step-growth polymerization of inorganic nanoparticles. *Science* **329,** 197–200 (2010).
24. Lvov, Y., Decher, G. & Möhwald, H. Assembly, structural characterization, and thermal behavior of layer-by-layer deposited ultrathin films of poly(vinyl sulfate) and poly(allylamine). *Langmuir* **9,** 481–486 (1993).
25. Billingsley, P. *Probability and Measure* 3rd edn (John Wiley & Sons, 1995).
26. Persson, A. E., Schoeman, B. J., Sterte, J. & Otterstedt, J. E. The synthesis of discrete colloidal particles of TPA-silicalite-1. *Zeolites* **14,** 557–567 (1994).
27. Distaso, M., Klupp Taylor, R. N., Taccardi, N., Wasserscheid, P. & Peukert, W. Influence of the counterion on the synthesis of ZnO mesocrystals under solvothermal conditions. *Chem. Eur. J.* **17,** 2923–2930 (2011).

28. Nishizawa, M., Menon, V. P. & Martin, C. R. Metal nanotubule membranes with electrochemically switchable ion-transport selectivity. *Science* **268,** 700–702 (1995).
29. Koktysh, D. S. *et al*. Biomaterials by design: layer-by-layer assembled ion-selective and biocompatible films of TiO_2 nanoshells for neurochemical monitoring. *Adv. Funct. Mater.* **12,** 255–265 (2002).
30. Ohara, P. C., Leff, D. V., Heath, J. R. & Gelbart, W. M. Crystallization of opals from polydisperse nanoparticles. *Phys. Rev. Lett.* **75,** 3466–3469 (1995).
31. Bolhuis, P. G. & Kofke, D. A. Monte Carlo study of freezing of polydisperse hard spheres. *Phys. Rev. E* **54,** 634–643 (1996).
32. Bates, M. A. & Frenkel, D. Influence of polydispersity on the phase behavior of colloidal liquid crystals: a Monte Carlo simulation study. *J. Chem. Phys.* **109,** 6193–6199 (1998).
33. Orlik, R., Mitus, A. C., Kowalczyk, B., Patashinski, A. Z. & Grzybowski, B. A. Computer simulation of self-assembly (crystallization) of oppositely charged nanoparticles with various size distributions. *J. Non-Cryst. Solids* **355,** 1360–1369 (2009).
34. Phillips, C. L., Iacovella, C. R. & Glotzer, S. C. Stability of the double gyroid phase to nanoparticle polydispersity in polymer-tethered nanosphere systems. *Soft Matter* **6,** 1693–1703 (2010).
35. Kalsin, A. M. *et al*. Electrostatic self-assembly of binary nanoparticle crystals with a diamond-like lattice. *Science* **312,** 420–424 (2006).
36. Warner, M. G. & Hutchison, J. E. Linear assemblies of nanoparticles electrostatically organized on DNA scaffolds. *Nature Mater.* **2,** 272–277 (2003).
37. Manchester, M. & Steinmetz, N. F. *Viruses and Nanotechnology* (Springer, 2009).
38. Feldheim, D. L. & Foss, C. A. *Metal Nanoparticles: Synthesis, Characterization, and Applications* (Marcel-Dekker, 2002).
39. Chen, T., Zhang, Z. L. & Glotzer, S. C. A precise packing sequence for self-assembled convex structures. *Proc. Natl Acad. Sci. USA* **104,** 717–722 (2007).

Acknowledgements

The authors thank the 100 Talents Program of the Chinese Academy of Sciences (Z.Y.T.), the National Natural Science Foundation for Distinguished Youth Scholars of China (21025310, Z.Y.T.) the National Research Fund for Fundamental Key Project no. 2009CB930401 (Z.Y.T.), National Natural Science Foundation of China (nos 91027011 and 20973047, Z.Y.T.). This material is based on work supported in part by the US Army Research Office (grant award no. W911NF-10-1-0518, S.C.G. and N.A.K.). S.C.G. and T.D.N. also acknowledge support from the James S. McDonnell Foundation 21st Century Science Research Award/Studying Complex Systems (award no. 220020139). This material is based on work supported by the Department of Defense, Office of the Director, Defense Research and Engineering (DOD/DDRE) (award no. N00244-09-1-0062, S.C.G.). Any opinions, findings, and conclusions or recommendations expressed in this publication are those of the author(s) and do not necessarily reflect the views of the DOD/DDRE. Use of the Advanced Photon Source, an Office of Science User Facility operated for the US Department of Energy (DOE) Office of Science by Argonne National Laboratory, was supported by the US DOE (contract no. DE-AC02-06CH11357). This material is based on work partially supported by the Center for Solar and Thermal Energy Conversion, an Energy Frontier Research Center funded by the US DOE, Office of Science, Basic Energy Sciences (award no. DE-SC0000957, N.A.K.). The authors acknowledge support from the National Science Foundation (grant nos ECS-0601345, EFRI-BSBA 0938019, CBET 0933384 and CBET 0932823, N.A.K.). Any opinions, findings, and conclusions or recommendations expressed in this material are those of the authors and do not necessarily reflect the views of the NSF. The work is also partially supported by NIH 1R21CA121841-01A2 (NAK). S.C.G. is grateful to the University of Michigan Center for Advanced Computing for cluster support. The authors thank the University of Michigan's EMAL for its assistance with electron microscopy, and for NSF grant no. DMR-9871177 for funding for the JEOL 2010F analytical electron microscope used in this work. T.D.N. acknowledges support from the Vietnam Education Foundation. B.L. thanks the Argonne National Laboratory for use of the APS. Work at the Center for Nanoscale Materials was supported by the Office of Science, Office of Basic Energy Sciences, of the US DOE (contract no. DE-AC02-06CH-11357). P.P. acknowledges the support of a Willard Frank Libby postdoctoral fellowship from Argonne National Laboratory.

Author contributions

Y.S.X., Z.Y.T., and N.A.K. conceived and designed the experiments. Y.S.X. performed the experiments. T.D.N., A.S. and S.C.G. designed and performed the computer simulations. B.L. and P.P. carried out SAXS measurements and corresponding data analysis. M.Y. contributed to the nanoparticle synthesis. Y.S.X., T.D.N., B.L., Z.Y.T., S.C.G. and N.A.K. analysed the data. Y.S.X., T.D.N., B.L., Z.Y.T., S.C.G. and N.A.K. co-wrote the paper. All authors discussed the results and commented on the manuscript.

Additional information

The authors declare no competing financial interests. Supplementary information accompanies this paper at www.nature.com/naturenanotechnology. Reprints and permission information is available online at http://www.nature.com/reprints. Correspondence and requests for materials should be addressed to Z.T., S.C.G. and N.A.K.

ERRATUM

Self-assembly of self-limiting monodisperse supraparticles from polydisperse nanoparticles

Yunsheng Xia, Trung Dac Nguyen, Ming Yang, Byeongdu Lee, Aaron Santos, Paul Podsiadlo, Zhiyong Tang, Sharon C. Glotzer and Nicholas A. Kotov

Nature Nanotechnology http://dx.doi.org/10.1038/nnano.2011.121 (2011); published online 21 August 2011; corrected online 26 August 2011.

In the version of this Article originally published online, the full list of corresponding authors should have been Zhiyong Tang, Sharon C. Glotzer and Nicholas A. Kotov. This has been corrected in all versions of the Article.